Macromolecules

COMMUNICATION TO THE EDITOR

pubs.acs.org/Macromolecules

Enhanced Charge-Carrier Mobility in High-Pressure-Crystallized Poly(3-hexylthiophene)

Christian Müller,[$,†] Nikolai D. Zhigadlo,[‡] Avinesh Kumar,[§] Mohammed A. Baklar,[§,∥] Janusz Karpinski,[‡] Paul Smith,[†,⊥] Theo Kreouzis,[‡] and Natalie Stingelin*[,∥,⊥,#]

[†]Department of Materials, ETH Zurich, Zurich, Switzerland

[‡]Laboratory for Solid State Physics, ETH Zurich, Zurich, Switzerland

[§]Centre for Materials Research, Queen Mary University of London, London, United Kingdom

[∥]Department of Materials, Imperial College London, London, United Kingdom

[⊥]Centre for Plastic Electronics, Imperial College London, London, United Kingdom

[#]FRIAS, School of Soft Matter Research, University of Freiburg, Freiburg, Germany

Supporting Information

Polymeric organic semiconductors, like many other macromolecular systems, can display the full spectrum of microstructures, from essentially disordered, or amorphous, to highly crystalline. Many electronic properties and processes are critically depending on this molecular and supramolecular order.[1−4] However, it often is still unclear which particular microstructural aspects contribute to the macroscopic electronic attributes of these materials. In the field of commodity polymers, such as polyethylene (PE), isotactic polypropylene (*i*-PP), nylons, and polyesters, one structural characteristic that has been found to be of paramount importance for optimizing mechanical functionalities, including Young's modulus and, in particular, tensile strength, is the degree of chain extension and associated lamellar crystal thickness l (see for a schematic Figure 1a). In analogy, in the present study we focused on this specific feature and explored whether l, varied through different processing schemes, influences charge transport in conjugated polymeric matter. Initial indications for such a relation exist. On the basis of a range of poly(3-hexylthiophene)s (P3HT) of relatively low weight-average molecular weight M_w (2.4 kg mol^{-1} < M_w < 18 kg mol^{-1}), Zhang et al. have, for example, established a correlation between "weight-average contour length L_W" and field-effect transistor charge-carrier mobilities μ_{FET}, with μ_{FET} increasing with L_W.[5] Considering the relatively low molecular weight of the materials investigated by Zhang et al., one can assume from Brinkmann and Rannou's work that these P3HTs form chain extended crystals, which would imply that $L_W \sim l$.

Here, we focus on P3HTs of larger molecular weights to ensure that the macromolecules are of a length well above the range where they naturally form extended-chain crystals, i.e., in the regime where chain folding sets in, and chain entanglements form in their melt or concentrated solutions (schematically indicated in Figure 1b; see also refs 6−11). Two different P3HTs (weight-average molecular weight M_w = 60 and 344 kg mol^{-1}) were selected and solidified from the melt at ambient and under elevated pressure. For comparison, both polymers were also cast from solution, as this is the most frequently adopted processing method for this polymer family. In addition, thin films were prepared from solution at ambient from a low-molecular-weight P3HT of M_w = 22 kg mol^{-1}, which does not feature molecularly connected crystalline moieties and can be expected to form chain extended crystals also when processed at ambient conditions. The latter is evident from their brittle tensile behavior (Supporting Information Table S1). [N.B. We observe the onset of plastic deformation for the material of M_w = 60 kg mol^{-1}, indicating that elastic percolation is reached. This implies that the crystalline entities are connected through individual macromolecules ("tie molecules"; see schematic in Supporting Information Figure S1), which results in the typical structure of common semicrystalline "plastics" of alternating crystalline lamellae and amorphous (largely unordered) regions, as they are processed at ambient from the melt or concentrated solutions.[6,12]]

Standard protocols were followed for solution- (2 wt % P3HT in xylene) and melt-crystallization at ambient.[13−15] Pressure-induced solidification was performed in a cubic anvil press. More specifically, 0.1 g of P3HT was heated in a boron nitrite (BN) crucible inside a pyrophyllite cube with a graphite heater from room temperature to ∼300 °C at ambient pressure, at a rate of 10 °C min^{-1}. Subsequently, the pressure on the assembly was increased from ambient to 5 kbar at a rate of 0.33 kbar min^{-1} through use of six tungsten carbide anvils. Thereafter, the polymer was cooled to room temperature at 10 °C min^{-1} under 5 kbar, followed by release of the pressure. [N.B. These processing parameters were selected based on the fact that for most polymers featuring weak secondary van der Waals bonding (such as P3HT) application of a pressure of 5 kbar results in an increase in their melting temperature T_m by ∼100 °C,[16−20] thereby creating a pressure-induced supercooling, which in turn causes the phenomenon of pressure-induced solidification.[6]]

The above experimental procedure resulted in dense cubes of P3HT of a few mm^3 in size, which were of a conspicuous golden appearance and featured characteristic striations generally observed for extended-chain crystals,[6] as the photograph in Figure 1c illustrates. Of note is that the crystal unit cell of these

Received: November 20, 2010
Revised: January 22, 2011
Published: February 04, 2011

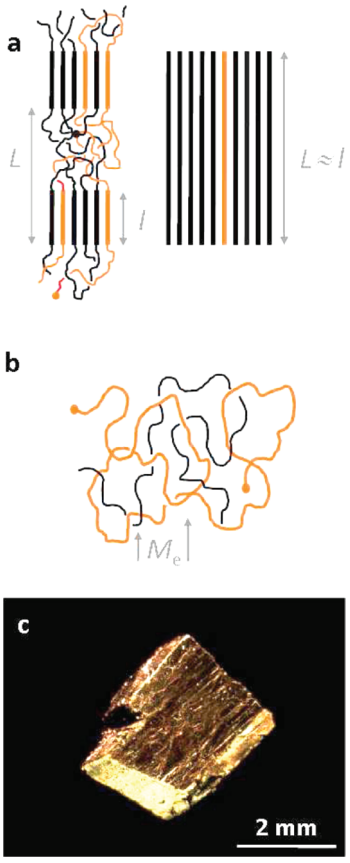

Figure 1. (a) Depending on the experimental conditions under which polymers solidify, a variety of structures can be obtained that comprise crystalline building blocks similar to those found in single crystals. Characteristic periodicities, i.e., the long period L and the lamellar crystal thickness l, are indicated in the left panel. Fully extended structures may be obtained if the chain length (i.e., the molecular weight) is sufficiently small or the density of entanglements is reduced prior to solidification by selection of suitable processing routes. (b) Schematic of a polymer melt or polymer solution of high concentration. The molecular weight between two entanglements M_e is indicated. (c) Photograph of a P3HT sample (M_w = 344 kg mol^{-1}) solidified at 5 kbar.

materials was unaltered; i.e., application of a high pressure of 5 kbar appeared not to induce another crystal polymorph, as evidenced by the wide-angle X-ray diffractograms presented in Figure 2. Thus, from a crystallographic perspective, the high-pressure-solidified samples are comparable to solution- and melt-crystallized material. However, the (100) reflection (q = 0.399 Å^{-1}) was found to be more intense for the high-pressure-solidified specimen when compared with solution- and melt-crystallized (at ambient pressure) samples. This finding is indicative of an increased degree of crystallinity of the former.

This conclusion is supported by differential scanning calorimetry (DSC) studies. Significantly higher enthalpies of fusion ΔH_f were recorded for the high-pressure-solidified materials ($\Delta H_f^{\text{high-pressure}} \approx 30$ J g^{-1} vs $\Delta H_f^{\text{melt-crystallized}} \approx 23$ J g^{-1} for P3HT^{60K}, and $\Delta H_f^{\text{high-pressure}} \approx 29$ J g^{-1} vs $\Delta H_f^{\text{melt-crystallized}} \approx 17$ J g^{-1} for P3HT^{344K}; see Table 1 and Figure 3a). These values correspond to a degree of bulk crystallinity of 30% (28%) and 23% (17%) for respectively pressure- and ambient melt-solidified P3HT of M_w = 60 kg mol^{-1} (344 kg mol^{-1}), assuming an enthalpy of fusion for a 100% crystalline materials ΔH_f° = 99 J g^{-1} (with $X = \Delta H_f/\Delta H_f^\circ$).[21]

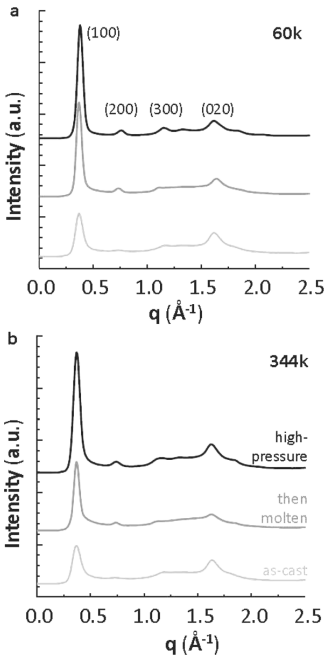

Figure 2. Wide-angle X-ray diffractograms of P3HTs crystallized from the melt at ambient pressure (dark gray pattern) and at 5 kbar (black) and from solution at ambient (light gray). (a) P3HT of M_w = 60 kg mol^{-1}; (b) P3HT of M_w = 344 kg mol^{-1}. [Data for P3HT structures produced at ambient were obtained from the same film, which was first cast and then analyzed, after which it was molten, solidified, and remeasured.]

Table 1. Microstructural Data Deduced from Small-Angle X-ray Scattering, Wide-Angle-X-ray Dffraction, and Differential Scanning Calorimetry for Poly(3-hexylthiophene) (P3HT) of M_w = 60 and 344 kg mol^{-1}, Melt-Crystallized at Ambient Pressure and 5 kbar

P3HT grade[protocol]	q, nm^{-1}	long period L, nm	crystallinity X, %	lamellar thickness l, nm
60K$^{\text{melt}}$	0.3	21	23	4.9
60K$^{\text{high-pressure}}$	0.3	19	30	5.8
344 K$^{\text{melt}}$	0.2	31	17	5.4
344 K$^{\text{high-pressur}}$	0.2	31	28	8.9

More strikingly, though, the calorimetric studies revealed a distinct increase of the melting temperature T_m of the high-pressure-crystallized polymer, from 235 to 248 °C for P3HT of M_w = 60 kg mol^{-1} and 240 to 252 °C for the 344 kg mol^{-1} material, compared to the identical species solidified from the melt at ambient (Figure 3a and Table 1). This increase in melting temperature of high-pressure-solidified P3HT is suggestive of a larger lamellar crystal thickness and a partial chain extension in these materials (schematically depicted in Figure 1a, right), as a correlation between T_m and l is well-known and well established.[6,10,22−24]

We, therefore, set out to generate more quantitative information regarding the thickness of the crystalline entities constituting the various P3HT solids. For this purpose, we employed small-angle X-ray scattering (SAXS; for experimental methods see ref 25). In Figure 3b, the SAXS profiles of both high-pressure-solidified material and P3HT melt-crystallized at ambient are

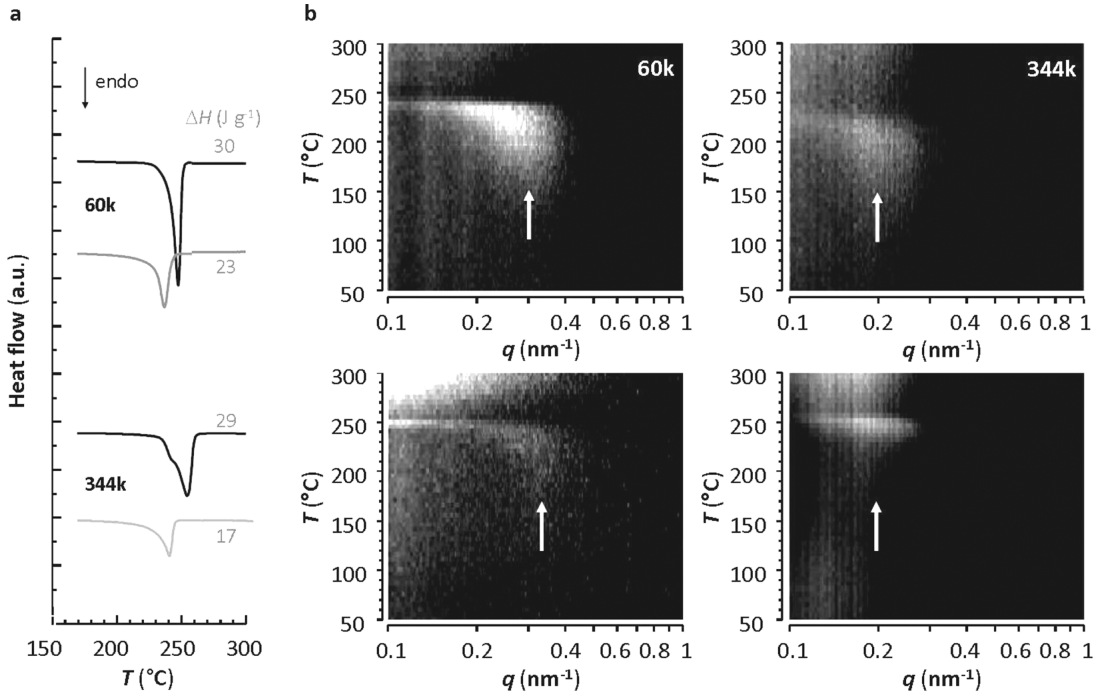

Figure 3. (a) Differential scanning calorimetry of P3HT of M_w = 60 kg mol^{-1} (top panel) and 344 kg mol^{-1} (bottom panel). Material solidified at 5 kbar (black) and crystallized from the melt at ambient pressure (gray). (b) Small-angle X-ray patterns for the two respective polymers (P3HT of M_w = 60 kg mol^{-1}: left panel; M_w = 344 kg mol^{-1}: right panel). Top: P3HT crystallized at ambient. Bottom: at high pressure. Average long periods, as deduced from peak intensities in the SAXS profiles, are indicated with arrows.

shown. Employing these data, average long periods L (i.e., the periodicity of a lamellar crystalline stack *and* amorphous interlamellar phase; cf. Figure 1a, left) were deduced from the peak positions indicated with arrows in Figure 2b. Values of L were found to be of similar magnitude (~20 nm for the P3HT of M_w = 60 kg mol^{-1} and ~30 nm for the polymer of M_w = 344 kg mol^{-1}) in both the high-pressure and the melt-solidified materials and were in the range previously reported for other P3HTs.[24,26] As a matter of fact, Wu et al. reported long periods of 27 nm for P3HTs of M_w = 21 kg mol^{-1},[26] and Canetti et al. found L to be in the range of 11.7 and 16.8 nm for systems of $M_w \approx 16$ kg mol^{-1},[24] depending on the annealing protocol followed,[23] both in agreement with the transmission electron microscopy data reported by Brinkmann and Rannou.[13] Taking into account the difference in degree of crystallinity X of our P3HT samples (melt-crystallized at high vs ambient pressure), we arrived at the conclusion that pressure-induced crystallization resulted in an increase of the crystal thickness $l = (\Delta H_f/\Delta H_f^\circ)L = XL$ of up to 65% for the higher molecular weight material ($l^{\text{melt-solidified}} \approx 5.4$ nm to $l^{\text{high-pressure}} \approx 8.9$ nm), while an increase of more than 15% was observed for the P3HT of M_w = 60 kg mol^{-1} ($l^{\text{melt-solidified}} \approx$ 4.9 nm; $l^{\text{high-pressure}} \approx 5.8$ nm).

Further exploring the above-mentioned correlation between crystal thickness and T_m, we adopted the commonly applied Gibbs−Thomson equation,[27] which for polymers generally is presented in the form of

$$T_m = T_m^\circ[1-[2\gamma/(\Delta H_f l)] \quad (1)$$

where T_f° is the equilibrium melting temperature, ΔH_f the enthalpy of fusion per unit volume, γ the lamellar surface free energy (or "fold-surface" free energy), and l the lamellar crystal thickness. Extrapolating the increase in T_m found for high-pressure-solidified material to the melting point of P3HT crystals of *infinite* size T_m°,[27] we find for the P3HT of M_w = 344 kg mol^{-1} T_m° to be >270 °C. Note that this value is slightly higher than previously reported for P3HT by Canetti et al.[24] We attribute this discrepancy to the higher molecular weight of the P3HT we used for our study—a relation which has been quantitatively described by Flory and Vrij.[28]

From the above microstructural analysis, we conclude that pressure-induced solidification indeed caused formation of P3HT solids not only of higher degrees of bulk crystallinity but also of increased crystal thickness. We now turn to the electronic characteristics of such P3HT samples and their dependence on these structural features. To this end, the bulk charge-transport properties of P3HT samples were assessed by time-of-flight (TOF) photoconductivity measurements (Figure 4). Dispersive hole photocurrent transients similar to those reported previously for solution-processed P3HT[13] were found for all our materials; however, the inflection point arrival times t_t (indicated in Figure 4a with arrows) differed considerably. Remarkably indeed, for the high-molecular-weight P3HT, the transient arrival time t_t (at electric field $E = 10^5$ V s^{-1}) decreased by more than 2 orders magnitude from close to 10^5 μs to less than 10^3 μs, as is evident from Figure 4a. The latter, faster transport corresponds to an improvement in charge-carrier mobility μ_{TOF} of close to 100 (Figure 4b, circles), as deduced from the expression

$$\mu_{TOF} = d^2/Vt_t \quad (2)$$

where d is the sample thickness, t_t the inflection point arrival time obtained from a double-logarithmic plot of the photocurrent transient (see Figure 4a), and V the applied voltage.

For the lower-molecular-weight material (60 kg mol^{-1}), the enhancement in charge-carrier mobility in pressure solidified

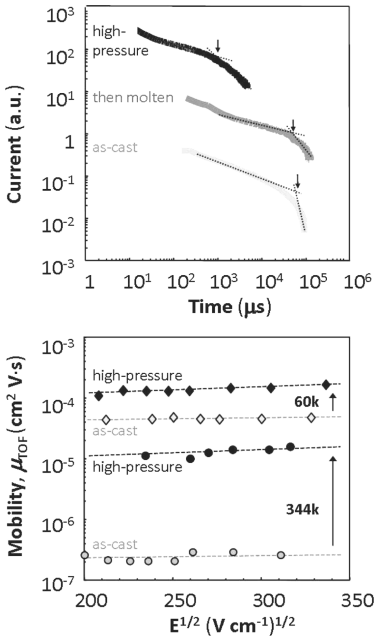

Figure 4. (a) Time-of-flight (TOF) photoconductivity transients for P3HT of M_w = 344 kg mol^{-1}, crystallized from solution (light gray) and the melt (dark gray: solidified at ambient pressure; black: solidified at 5 kbar). Transient arrival times t_t are indicated with arrows. Again the same film was used for characterization of samples produced at ambient. (b) Field dependence of TOF charge-carrier mobility. A comparison between high-pressure-solidified (black symbols) P3HT and material-crystallized from solution (light gray symbols) is shown (square symbols: P3HT^{60K}; circles: P3HT^{344K}). [Note: the electronic response time of the circuit τ was at all times kept well below the time base of the measurement.]

materials was less pronounced (Figure 4b, square symbols). According to classical polymer science, such behavior may have been expected as polymers of shorter length (lower molecular weight) more readily form extended chain crystals and, hence, benefit less from pressure-induced formation of solids. This insight is further supported by the fact that the high-pressure-solidified P3HT of M_w = 60 kg mol^{-1} displayed essentially identical time-of-flight mobility values as material of M_w = 22 kg mol^{-1} cast from solution at ambient (see Supporting Information Figure S2). As discussed above, the latter sample will feature a chain-extended solid-state microstructure, indicating that a saturation in μ_{TOF} has been reached. The latter observations is also in accord with work by Ballantyne et al.,[29] who showed that the time-of-flight mobility increases with decreasing M_w, leveling off around a value $\mu_{TOF} \sim 1 \times 10^{-4}$ cm^2 V^{-1} s^{-1} at $M_w \sim 20$ kg mol^{-1}.

Questions remain why we find improved bulk charge-transport in high-pressure-solidified materials. While thermal analysis, in combination with wide-angle X-ray diffraction and small-angle X-ray scattering, strongly implies that the lamellar crystal thickness in P3HT structures can be increased through pressure-induced crystallization, clearly also their overall degree of crystallinity was enhanced (see Table 1). Therefore, it may be difficult to fully disentangle the effects of these two microstructural aspects on charge-transport properties. Indeed, in the P3HT investigated here the material of M_w = 60 kg mol^{-1} (high-pressure solidified) displayed higher TOF moblities than the material of M_w = 344 kg mol^{-1} processed in the same manner, despite the latter featured crystalline lamellae of higher values of l. This probably is due to a number of reasons: P3HT of M_w = 60 kg mol^{-1} is possibly chemically more pure and of lower polydispersity, but it is also more crystalline. A more fair comparison may be based on systems of similar—if not identical—M_w. For instance, in recent work we have shown that blends of P3HT with high-density polyethylene (HDPE) resulted in a considerably improved bulk charge transport, while the degree of crystallinity of the semiconductor in such binaries was not significantly affected.[13] A noticeable increase in melting temperature was observed, however, for these semiconducting:insulating systems, which suggests that crystals of increased thickness and more extended chain structures were obtained through the blending procedure, resulting in the observed enhanced electronic properties.

In summary, our data strongly indicates that the lamellar crystal thickness can influence the electronic properties of conjugated polymers of $M_w \gg M_e$. Therefore, further improvements in these characteristics may be possible when employing the necessary physicochemical means to fully extent high-molecular-weight polymer semiconductors during assembly of the solid state. Intuitively, high-pressure solidification is not likely to be the appropriate tool for this purpose, especially for fabrication of architectures for commercial usage, but results obtained with the above-mentioned P3HT:HDPE blends illustrate that various other means exist that permit tailoring specific structural characteristic of functional materials of polymeric nature. Advantageous alternative pathways toward increased crystal thickness are, of course, crystallization at elevated temperature from dilute solutions, or the so-called "virgin" processing routes. The latter takes advantage of the observation that under favorable thermodynamic/kinetic conditions during their creation macromolecules can be retrieved from the reactor in a solid form that is highly ordered ("crystalline") and in which the polymer chains are virtually free of chain entanglements and thus can be processed directly in highly extended chain structures.[30−32]

■ ASSOCIATED CONTENT

Supporting Information. Experimental details, Table S1, and Figures S1 and S2. This material is available free of charge via the Internet at http://pubs.acs.org.

■ AUTHOR INFORMATION

Corresponding Author

*E-mail: natalie.stingelin@imperial.ac.uk.

Present Addresses

[$]Department of Physics, Chemistry & Biology, Linköping University, Linköping, Sweden.

■ ACKNOWLEDGMENT

This research was funded by the European Community's Seventh Framework Programme (FP7/2007-2013) under grant agreement no. 212311 of the ONE-P project. N.S. in addition acknowledges support from UK's Engineering and Physical Sciences Research Council (EPSRC) EP/G060738/1. The authors extend their thanks to ESRF (Dubble Beamline) for their assistance with the SAXS experiments and to Merck Chemicals, Prof. Iain McCulloch, and Dr. Martin Heeney

(Department of Chemistry, Imperial College London) for their generous supply of P3HT.

REFERENCES

(1) Chang, J.-F.; Sun, B.; Breiby, D. W.; Nielsen, M. M.; Sölling, T. I.; Giles, M.; McCulloch, I.; Sirringhaus, H. *Chem. Mater.* **2004**, *16*, 4772–4776.
(2) Clark, J.; Chang, J.-F.; Spano, F. C.; Friend, R. H.; Silva, C. *Appl. Phys. Lett.* **2009**, *94*, 163306.
(3) Jimison, L. H.; Toney, M. F.; McCulloch, I.; Heeney, M.; Salleo, A. *Adv. Mater.* **2009**, *21*, 1568–1572.
(4) Sirringhaus, H.; Wilson, R. J.; Friend, R. H.; Inbasekaran, M.; Wu, W.; Woo, E. P.; Grell, M.; Bradley, D. D. C. *Appl. Phys. Lett.* **2000**, *77*, 406–408.
(5) Zhang, R.; Li, B.; Iovu, M. C.; Jeffries-EL, M.; Sauvé, G.; Cooper, J.; Jia, S.; Tristram-Nagle, S.; Smilgies, D. M.; Lambeth, D. N.; McCullough, R. D.; Kowalewski, T. *J. Am. Chem. Soc.* **2006**, *128*, 3480–3481.
(6) Wunderlich, B. *Macromolecular Physics*; Academic Press: New York, 1976; Vol. 2.
(7) De Gennes, P. G. *Scaling Concepts in Polymer Physics*; Cornell University Press: Ithaca, NY, 1979.
(8) Brinkmann, M.; Rannou, P. *Macromolecules* **2009**, *42*, 1125–1130.
(9) Kline, R. J.; McGehee, M. D.; Kadnikova, E. N.; Liu, J.; Fréchet, J. M. J.; Toney, M. F. *Macromolecules* **2005**, *38*, 3312–3319.
(10) Ungar, G.; Stejny, J.; Keller, A.; Bidd, I.; Whiting, M. C. *Science* **1985**, *229*, 386–389.
(11) Brinkmann, M.; Rannou, P. *Adv. Funct. Mater.* **2007**, *17*, 101–108.
(12) Virkar, A. A.; Mannsfeld, S.; Bao, Z.; Stingelin, N. *Adv. Mater.* **2010**, *22*, 3857–3875.
(13) Kumar, A.; Baklar, M. A.; Scott, K.; Kreouzis, T.; Stingelin-Stutzmann, N. *Adv. Mater.* **2009**, *21*, 4447–4451.
(14) Müller, C.; Radano, C. P.; Smith, P.; Stingelin-Stutzmann, N. *Polymer* **2008**, *49*, 3973–3978.
(15) Inganäs, O.; Gustafsson, G.; Svensson, C. *Synth. Met.* **1991**, *41*−*43*, 1095–1101.
(16) McGeer, P. L.; Duus, H. C. *J. Chem. Phys.* **1952**, *20*, 1813–1814.
(17) Baer, E.; Kardos, J. L. *J. Polym. Sci., Part A* **1965**, *3*, 2827–2841.
(18) Davidson, T.; Wunderlich, B. *J. Polym. Sci., Part A-2* **1969**, *7*, 377–388.
(19) Nelson, R. R.; Webb, W.; Dixon, J. A. *J. Chem. Phys.* **1960**, *33*, 1756–1764.
(20) Yoshino, K.; Nakao, K.; Onoda, M.; Sugimoto, R. *Solid State Commun.* **1988**, *68*, 513–516.
(21) Malik, S.; Nandi, A. K. *J. Polym. Sci., Part B: Polym. Phys.* **2002**, *40*, 2073–2085.
(22) Prime, R. B.; Wunderlich, B. *J. Polym. Sci., Part A-2* **1969**, *7*, 2061–2072.
(23) Rees, D. V.; Bassett, D. C. *J. Polym. Sci., Part A-2* **1971**, *9*, 385–406.
(24) Canetti, M.; Bertini, F.; Scavia, G.; Porzio, W. *Eur. Polym. J.* **2009**, *45*, 2572–2579.
(25) Bras, W.; Dolbnya, I. P.; Detollenaere, D.; van Tol, R.; Malfois, M.; Greaves, G. N.; Ryan, A. J.; Heeley, E. *J. Appl. Crystallogr.* **2003**, *36*, 791–794.
(26) Wu, Z.; Petzold, A.; Henze, T.; Thurn-Albrecht, T.; Lohwasser, R. H.; Sommer, M.; Thelakkat, M. *Macromolecules* **2010**, *43*, 4646–4653.
(27) Wunderlich, B.; Czornyj, G. *Macromolecules* **1977**, *10*, 906–913.
(28) Flory, P. J.; Vrij, A. *J. Am. Chem. Soc.* **1963**, *85*, 3548–3553.
(29) Ballantyne, A. M.; Chen, L.; Dane, J.; Hammant, T.; Braun, F. M.; Heeney, M.; Duffy, W.; McCulloch, I.; Bradley, D. D. C.; Nelson, J. *Adv. Funct. Mater.* **2008**, *18*, 2373–2380.
(30) Starkweather, H. W., Jr. *Macromolecules* **1986**, *19*, 1131–1134.
(31) Ebnesajjad, S. *Fluoroplastics*; Plastics Design Library: Norwich, NY, 2000; Vol. 1, pp 168−184.
(32) Rotzinger, B. P.; Chanzy, H. D.; Smith, P. *Polymer* **1989**, *30*, 1814–1819.